

orites. If trapped noble gases in EET79001 were derived from the martian atmosphere, they may have been accompanied by ~ 0.1 part per million (ppm) N_2 and ~ 5 ppm CO_2 (15). It will be important to determine the $^{15}N/^{14}N$ ratio in EET79001 because of the large difference between martian and terrestrial N_2 isotopic compositions (15). Isotopic measurements of N_2 and CO_2 at these concentrations, however, will be difficult to make.

The presence of trapped martian atmosphere in EET79001, if corroborated by further studies on nonnoble gases, would be a particularly strong argument for the idea that this meteorite is from Mars. The dynamical mechanism required to remove material from a planetary-sized body remains uncertain, although specific mechanisms have been suggested (22). The recent identification of another Antarctic meteorite with a probable lunar origin (23) suggests that such mechanisms exist. A potential to associate readily available meteoritic material with the martian surface is yet one more demonstration of the value of analytical studies of meteorites to planetary science.

D. D. BOGARD
P. JOHNSON

Planetary and Earth Sciences
Division, NASA Johnson Space
Center, Houston, Texas 77058

References and Notes

1. E. M. Stolper and H. Y. McSween, *Geochim. Cosmochim. Acta* **43**, 1475 (1979); ———, J. F. Hays, *ibid.* **42**, 589 (1978).
2. G. Dreibus *et al.*, *Lunar Planet. Sci.* **13**, 186 (1982).
3. R. N. Clayton and T. K. Mayeda, *Earth Planet. Sci. Lett.*, in press.
4. C. Y. Shih *et al.*, *Geochim. Cosmochim. Acta* **46**, 2323 (1982).
5. N. Nakamura, D. M. Unruh, M. Tatsumoto, R. Hutchison, *ibid.*, p. 1555.
6. N. Nakamura, H. Kagami, H. Koni, *Meteoritics*, in press; J. L. Wooden *et al.*, *Lunar Planet. Sci.* **10**, 1379 (1979); N. H. Gale, J. W. Arden, R. Hutchison, *Earth Planet. Sci. Lett.* **26**, 195 (1975); F. A. Podosek, *ibid.* **19**, 135 (1973); D. D. Bogard and L. Husain, *Geophys. Res. Lett.* **4**, 69 (1977); D. A. Papanastassiou and G. J. Wasserburg, *ibid.* **1**, 23 (1974).
7. H. Y. McSween and E. M. Stolper, *Sci. Am.* **242** (No. 6), 54 (1980); J. T. Wasson and G. W. Wetherill, *Asteroids* (Univ. of Arizona Press, Tucson, 1979), p. 926; L. E. Nyquist *et al.*, *Meteoritics* **14**, 502 (1979).
8. H. Y. McSween, Jr., L. A. Taylor, E. M. Stolper, *Science* **204**, 1201 (1979); M. S. Ma, J. C. Laul, R. A. Schmitt, *Proc. Lunar Planet. Sci. Conf.* **12**, 1349 (1981).
9. C. A. Wood and L. D. Ashwal, *Proc. Lunar Planet. Sci. Conf.* **12**, 1359 (1981).
10. W. A. Cassidy, *Antarct. J. U.S.* **15**, 49 (1980).
11. H. Y. McSween and E. Jarosewich, *Lunar Planet. Sci.* **13**, 503 (1982).
12. J. Wooden *et al.*, *ibid.*, p. 879.
13. H. Y. McSween and A. M. Reid, *Meteoritics* **16**, 359 (1981).
14. D. D. Bogard, in preparation.
15. T. Owen *et al.*, *J. Geophys. Res.* **82**, 4635 (1977).
16. E. Anders and T. Owen, *Science* **198**, 453 (1977).
17. R. A. Canals, E. C. Alexander, O. K. Manuel, *J. Geophys. Res.* **73**, 3331 (1968); F. P. Fanale and W. A. Cannon, *Earth Planet. Sci. Lett.* **11**, 362 (1971); ———, T. Owen, *Geophys. Res. Lett.* **5**, 77 (1978).

18. F. A. Podosek, M. Honda, M. Ozima, *Geochim. Cosmochim. Acta* **44**, 1875 (1980).
19. B. C. Clark and D. C. Van Hart, *Icarus* **45**, 370 (1981).
20. L. Schultz and H. Kruse, *Nucl. Track Detection* **2**, 65 (1978); R. O. Pepin and P. Signer, *Science* **149**, 253 (1965).
21. K. Fredriksson, P. DeCarli, R. O. Pepin, J. H. Reynolds, G. Turner, *J. Geophys. Res.* **69**, 1403 (1964); P. K. Davis, *Geochim. Cosmochim. Acta* **41**, 195 (1977).
22. L. E. Nyquist, *Proc. 13th Lunar Planet. Sci.*

- Conf. [J. Geophys. Res.* **88**, (Suppl.), A785 (1982)]; A. Singer, *Eos* **63**, 1020 (1982).
23. Papers presented at the Special Session on Meteorites from the Earth's Moon, Lunar and Planetary Science Conference, Lunar and Planetary Institute, Houston, 17 March 1983.
 24. E. Mazor, D. Heymann, E. Anders, *Geochim. Cosmochim. Acta* **34**, 781 (1970).
 25. We thank several of our colleagues, especially L. Nyquist, for constructive comments.

13 December 1982; revised 4 April 1983

Nuclear Magnetic Resonance Blood Flow Measurements in the Human Brain

Abstract. *Timed sequences of nuclear magnetic resonance imaging signals in the human head were used to quantitatively measure blood flow in the internal jugular veins. The procedure can be straightforwardly applied to any vein or artery in the body.*

In this report we describe the use of nuclear magnetic resonance (NMR) techniques to measure blood flow in the human head. In 1959 Singer (1) used NMR techniques to study blood flow in mouse tails, and in 1970 Morse and Singer (2) obtained NMR measurements of superficial venous flow in humans. Now we can combine NMR imaging systems (3) with the measurements of blood flow. The method will be described for two specific vessels in the human head, but it is suitable for any set of arteries or veins or even for blood perfusion measurements.

The procedure for blood flow imaging is as follows. The body is placed in a homogeneous magnetic field. It takes approximately 5 seconds for the protons in the body to be fully magnetized along the magnetic field. A specific volume V of the body is selected for flow imaging. A planar cross-sectional volume perpendicular to the flow vessels of interest is the appropriate choice. The selected volume is magnetically depolarized with a radio-frequency (RF) pulse. The RF pulse may be one of several types. We use a pulse to tip the protons in the plane by 90° and follow the pulse with a magnetic field gradient pulse to randomize the proton magnetic orientations in the selected volume. The randomization could also be carried out with a saturating pulse and, in some special procedures, with a 180° pulse. We will refer to all these randomization procedures as the depolarization pulse. After a selected specific time $t(x)$ a second RF pulse is provided. The second pulse tips all the fresh blood protons that entered the selected plane during the time $t(x)$ by 90° . The second pulse also tips the recovered protons that remain in the plane. The tipped magnetic blood protons and recovered stationary protons are then imaged by a spin echo technique (4-6), to provide picture elements (pixels) of flow information. Each pixel provides a voltage directly proportional to the volume of blood that flowed into the volume V . The computer is programmed to sum the NMR voltages from each pixel in the selected blood vessel and add these voltages to provide the flow data. The tissue recovering from saturation in the volume V during the time $t(x)$ gives an imaging signal. These signals do not interfere with the flow measurements because the flow vessels are clearly visualized in the image.

Table 1. Selected flow vessels with tabulated NMR signal intensities for various times of flow. Signal intensity values are proportional to the integrated NMR voltages over the vessel pixels. The data are plotted to evaluate the time required to fill the imaged volume of the vein with inflowing blood. Inflowing blood completely replaces outflowing depolarized blood in 330 msec in the left vein and in 273 msec in the right vein.

Flow time (msec)	Signal intensity	
	Left internal jugular vein	Right internal jugular vein
50	2341	2471
100	3267	3258
200	3885	4340
500	5325	5375

To obtain an accurate measurement of flow, the procedure is repeated several different times. For example, x can be 50, 100, 150, and 200 msec. With a computer program the volume flow rate can then be read out for a specific artery or vein. The integrated signals in the vessel are tabulated by the computer, integrated over the vessel area, and indexed with the specific time $t(x)$. The rate of flow of blood in any vessel (milliliters per second) is obtained by dividing

the volume of the vessel by the measured time to refill the vessel after the NMR depolarization pulse.

Measurements were carried out on the head of one of the authors (L.E.C.). The volume element v consists of a 7-mm-thick transverse section through a nose-ear plane (the posterior fossa plane). Figure 1 shows one of the NMR images illustrating the blood flow image with $x = 50$ msec. More specifically, the blue areas represent the blood flow due to 50 msec of polarized blood replacing the previously depolarized blood in the vessels.

Figure 1 shows the basilar part of the occipital bone as a central feature. To the right of the occipital bone are the internal and external jugular veins; the external jugular veins are closest to the ear. Other veins and arteries are also prominent by more blue than the surrounding tissue. Fat and bone marrow provide a larger NMR voltage signal in the images and are lighter in the color representation. The red-yellow regions correspond to smaller NMR signal amplitudes. The image is intensity-normalized in order to photographically reproduce more effectively. The relative NMR signal voltage level of each pixel is automatically registered and is stored in the computer memory.

To obtain the image we flipped and dispersed (or depolarized) all the tissue in a volume V , waited 50 msec, again flipped the tissue 90° , and then imaged only the blood that flowed into the vessels in the volume V during that 50 msec. Therefore, that image presents a snap-

Table 2. Computer-processed flow data for the internal jugular veins.

Quantity	Left internal jugular	Right internal jugular
Area (cm ²)	0.162	0.196
Mean diameter (cm)	0.45	0.50
Imaged length (cm)	0.7	0.7
Volume (cm ³)	0.113	0.137
Filling time (msec)	330	273
Mean velocity (cm/sec)	2.12	2.56
Flow rate (ml/sec)	0.344	0.501

shot of the volume of blood that flowed into V during 50 msec. This is termed the $t(50)$ image. In order to accurately measure blood flow in a selected vessel, the flow measurement pulse sequence is repeated with different values of $t(x)$, such as $x = 100, 200,$ and 500 msec for one measurement of flow.

The pixels representing the vessels, arteries, and veins show a localized, integrated NMR signal that grows with exposure time until reaching a maximum when the inflowing polarized blood replaces the magnetically saturated blood. This maximum can be determined by graphing the data.

Table 1 lists sequential intensities of NMR signals for various times of flow. The tabulation is of the NMR signal intensities in the internal jugular veins; however, any of the imaged vessels can be selected for computer tabulation of flow data. The data are used to generate a specific flow time parameter for the vessel of interest. The flow time parameter for a vessel is used to obtain a numer-

ical measurement of blood flow in the vessel.

The average cross-sectional area of the internal jugular veins was determined with a pixel-counting computer program (7). Vessel depth was known from the defined thickness of an imaging "slice," in this case 7 mm. The volume of the vein, $v(a)$, was thereby determined. The time required to fill the vein with polarized blood, $t(a)$, was obtained from the data in Table 1. The flow for the vein is therefore

$$Q = \frac{v(a)}{t(a)} \quad (1)$$

For the left and right internal jugular veins the pixel-counting procedure was used in conjunction with the imaging slice thickness of 7 mm. The resulting data are shown in Table 2. The flow in milliliters per second (Q) was obtained directly from the determination of $v(a)$ and $t(a)$ and from the application of Eq. 1. Flow velocity V was obtained from

$$V = QA \quad (2)$$

where A is the area of flow in a vessel.

Estimates of $v(a)$ and $t(a)$ can be programmed into a computer, and the arterial or venous flow rate can then be read out directly. Estimates of $v(a)$ were found by animal testing to be accurate within 5 percent. The error in determining $t(a)$ is due to uncertainties in interpolating the singular points of the data shown in Table 1. These singular points are found by computer analyses. If insufficient data are taken, then determination of the filling time for any vessel

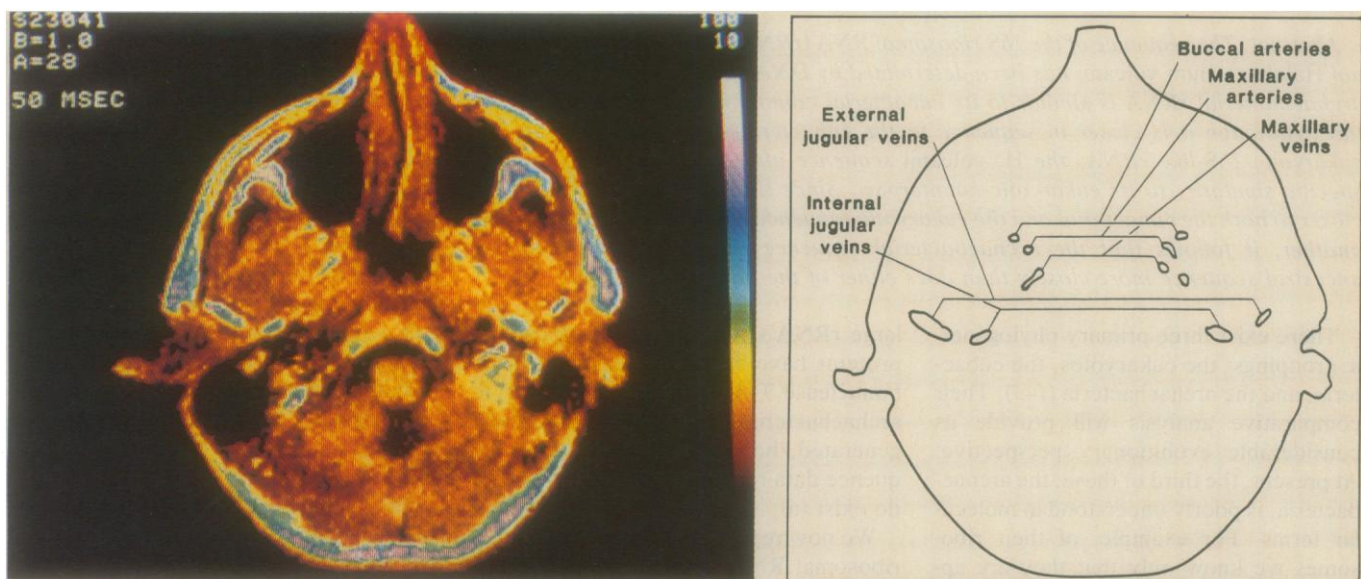


Fig. 1. Nuclear magnetic resonance image of a 7-mm-thick transverse section of Professor Crooks' brain through the posterior fossa (nose-ear) plane. The blood vessels (blue) show the intensities corresponding to 50 msec of blood flow. Blue represents higher-level NMR signals while red represents lower-level signals. [The blue signals in the peripheral regions are primarily due to fast T_1 (relaxation time) recoveries of peripheral fat tissue.] A timed sequence of images is required to obtain quantitative blood flow measurements for individual vessels.

involves some uncertainty. In essence, one can obtain more data and be more certain as to the accuracy of $t(a)$ for each vessel (8–10).

The relaxation time and the variations in carrying out 90° and 180° pulse timings are not significant sources of error because the procedure is iterative for each sequence of data. As a result, there is no linearity requirement in obtaining $t(a)$; instead one has only to observe the time at which the NMR signal of the flowing blood in the vessels stops increasing and remains constant. The error in $t(a)$ is therefore due to lack of sufficient data to measure the crossing points accurately. In the measurements we reported here, we estimate an overall accuracy of about 10 percent for the range of flows encountered.

Each of these measurements was averaged over 512 NMR signals. Each signal took approximately a half-second, so that, because of the averaging, about 4 minutes was given over to obtaining each set of pixels. Of course, all the points relating to 50 msec were obtained as a group, as were all the points relating to 100 msec, and so on. As a consequence, all the flow data for all the veins seen in an NMR image such as the one in Fig. 1 can be obtained in approximately 20 minutes. The computer can be programmed to obtain the flow data for the vessels in the selected slice and provide readouts simultaneously.

Sequence of the 16S Ribosomal RNA from *Halobacterium volcanii*, an Archaeobacterium

Abstract. *The sequence of the 16S ribosomal RNA (rRNA) from the archaeobacterium Halobacterium volcanii has been determined by DNA sequencing methods. The archaeobacterial rRNA is similar to its eubacterial counterpart in secondary structure. Although it is closer in sequence to the eubacterial 16S rRNA than to the eukaryotic 16S-like rRNA, the H. volcanii sequence also shows certain points of specific similarity to its eukaryotic counterpart. Since the H. volcanii sequence is closer to both the eubacterial and the eukaryotic sequences than these two are to one another, it follows that the archaeobacterial sequence resembles their common ancestral sequence more closely than does either of the other two versions.*

There exist three primary phylogenetic groupings: the eukaryotes, the eubacteria, and the archaeobacteria (1–3). Their comparative analysis will provide us considerable evolutionary perspective. At present, the third of these, the archaeobacteria, is poorly understood in molecular terms. For example, of their ribosomes we know only that they are approximately 30S and 50S in size and that their ribosomal RNA's (rRNA's) are slightly smaller than the corresponding eubacterial rRNA's (4). Neither of the

It has been proposed that NMR be used to study blood flow in the brain, heart, lungs, kidneys, and vascular system (8–10). We believe that the ability to visualize any vessel and quantitatively measure its blood flow will provide a means for monitoring the effectiveness of therapeutic treatments involving the vascular system.

J. R. SINGER

Department of Electrical Engineering and Computer Sciences, University of California, Berkeley 94720

L. E. CROOKS

Department of Radiology, University of California, San Francisco 94143

References and Notes

1. J. R. Singer, *Science* **130**, 1652 (1959).
2. O. C. Morse and J. R. Singer, *ibid.* **170**, 440 (1970).
3. L. Crooks *et al.*, *Radiology* **143**, 169 (April 1982).
4. E. L. Hahn, *Phys. Rev.* **80**, 580 (1950).
5. J. R. Singer and T. Grover, in *Modern Developments in Flow Measurements*, C. G. Clayton, Ed. (Peregrinus, London, 1972), pp. 38–44.
6. J. R. Singer, *J. Phys. E* **11**, 281 (1978).
7. L. Kaufman and W. Rowan, unpublished manuscript.
8. J. R. Singer, in *Nuclear Magnetic Resonance (NMR) Imaging*, C. L. Partain *et al.*, Eds. (Saunders, Philadelphia, 1983), pp. 168–178.
9. ———, in *Nuclear Magnetic Resonance Imaging in Medicine*, L. Kaufman, L. E. Crooks, A. R. Margulis, Eds. (Igaku-Shoin, New York, 1981), pp. 128–143.
10. J. M. Libove and J. R. Singer, *J. Phys. E* **13**, 38 (1980).
11. Supported in part by Dasonics, NMR, Inc., by PHS grant CA23850 from the National Cancer Institute, and by contract HV02928 from the National Heart, Lung, and Blood Institute. We thank L. Kaufman and A. Margulis for their support and encouragement.

2 February 1983; revised 29 April 1983

18S rRNA of eukaryotes. Yet in a number of details, it seems remarkably eukaryotic. In primary structure, the archaeobacterial 16S rRNA is closer to both its eubacterial and eukaryotic counterparts than these two are to one another.

Figure 1 shows the sequence of the *H. volcanii* 16S rRNA aligned with its counterparts from *Escherichia coli* and *Xenopus laevis*. The DNA sequence is completely consistent with the catalogs of oligonucleotides produced by digestion of the corresponding rRNA by ribonuclease T₁ (complete catalog, covering 47 percent of the sequence as pentamers or larger), by pancreatic ribonuclease (incomplete catalog), and by ribonuclease U₂ acting on RNA in which the G residues were blocked with glyoxal (incomplete catalog) (7). This indicates that no insertions of significant size occur in the gene. The RNA catalogs also permit identification of the functional termini of the 16S rRNA gene and placement of post-transcriptionally modified nucleotides.

The *H. volcanii* sequence, consisting of 1472 residues, is significantly shorter than its *E. coli* counterpart, which has 1542 residues (8). When the two sequences are optimally aligned (9), 59 percent of the positions in the *H. volcanii* sequence are identical to their counterparts in *E. coli* (8). This compares to 75 percent homology between *E. coli* 16S rRNA and that of the *Zea mays* chloroplast (10); these two rRNA's seem to represent the phylogenetic extremes within the eubacteria (2). The *H. volcanii* and *E. coli* sequences are very alike in secondary structure as well (see Fig. 2). Of the 50 odd secondary structural elements recognized in the *E. coli* sequence (9, 11), only three are absent in the *H. volcanii* version and an additional three or four are present in a somewhat altered form. The rest are virtually identical in the two cases; *H. volcanii* may have one or two helices not seen in its *E. coli* counterpart, but comparative proof for these is, at present, lacking. Furthermore, in all but a few of the homologous helical elements, the *H. volcanii* and *E. coli* versions differ in composition by replacements of at least two base pairs, providing additional support for the helices originally proposed on the basis of comparative studies within the eubacteria alone (11).

The degree of secondary structural resemblance between the two bacterial 16S rRNA's is greater than either shows with the eukaryotic 18S rRNA (*Xenopus laevis*) (9, 12). To understand how the three rRNA's are related, however, it is necessary to compare their sequences in